

Article

Controllable Introduction of Surface Defects on $\text{CH}_3\text{NH}_3\text{PbI}_3$ Perovskite

Sushu Wan ¹, Yajie Zhu ¹, Daocheng Hong ^{1,2} and Yuxi Tian ^{1,*}

¹ Key Laboratory of Mesoscopic Chemistry of MOE, Jiangsu Key Laboratory of Vehicle Emissions Control, School of Chemistry and Chemical Engineering, Nanjing University, Nanjing 210023, China; wansushu@outlook.com (S.W.); yajie.zhu@smail.nju.edu.cn (Y.Z.); hdaocheng@gmail.com (D.H.)

² Key Laboratory for Advanced Technology in Environmental Protection of Jiangsu Province, Yancheng Institute of Technology, Yancheng 224051, China

* Correspondence: tyx@nju.edu.cn

Abstract: One of the unique characteristics of semiconductors is the strong dependence of their properties on crystal defects and doping. However, due to the species diversity and low density, it is very difficult to control the type and concentration of the defects. In perovskite materials, crystal defects are randomly formed during the fast crystallization process, causing large heterogeneity of the samples. Here, in this work, we report a controllable method to introduce surface defects on $\text{CH}_3\text{NH}_3\text{PbI}_3$ perovskite materials via the interaction with 1,4-benzoquinone (BQ) molecules on the gas and solid interface. After the adsorption of BQ molecules on the perovskite surface, surface defects can be generated by photoinduced chemical reactions. The concentration of the defects can thus be controlled by precisely regulating the laser irradiation time. The concentration of the defects can be characterized by a gradually decreased PL intensity and lifetime and was found to influence the atmospheric response and the subsequent acetone-induced degradation of the materials. These results demonstrate that crystal defects in perovskite materials can be controllably introduced, which provides a possible way to fully understand the correlation between the nature and chemical structure of these defects.



Citation: Wan, S.; Zhu, Y.; Hong, D.; Tian, Y. Controllable Introduction of Surface Defects on $\text{CH}_3\text{NH}_3\text{PbI}_3$ Perovskite. *Nanomaterials* **2022**, *12*, 1002. <https://doi.org/10.3390/nano12061002>

Academic Editor: Aurora Rizzo

Received: 12 February 2022

Accepted: 16 March 2022

Published: 18 March 2022

Publisher's Note: MDPI stays neutral with regard to jurisdictional claims in published maps and institutional affiliations.



Copyright: © 2022 by the authors. Licensee MDPI, Basel, Switzerland. This article is an open access article distributed under the terms and conditions of the Creative Commons Attribution (CC BY) license (<https://creativecommons.org/licenses/by/4.0/>).

Keywords: lead halide perovskite; polycrystalline thin films; defect modification; defect concentration; optical microscopy

1. Introduction

Organometal halide perovskites have demonstrated prompt progress in optoelectronic devices [1], e.g., solar cells [2–4], light-emitting diodes [5] and lasers [6], thanks to their low-cost preparation method, suitable and tunable bandgap, high absorption coefficient and long charge diffusion length [7–11]. Accompanied by the remarkable increase in the power conversion efficiency (PCE) of perovskite solar cells (PSCs) [12], one main concern of its practical application is the instability of the devices outside the glove box [13]. To improve the device efficiency and lifetime, many strategies, including fabrication optimization [14,15], composition engineering [16,17] and surface passivation [18,19], have been taken, and the modification of defect properties plays an important role during those processes.

Although halide perovskite is reported to demonstrate a high defect tolerance [20,21], it is unavoidable to form deep defects during the solution processing, thus hindering the devices' PCE approaching the theoretical limit [22]. Aristidou et al. reported that iodine vacancies can mediate the formation of superoxide and induce the degradation of the materials [23]. Azpiroz et al. reported that defects can facilitate ion migration, causing hysteresis effects in PSCs [24]. Grain boundaries are especially vulnerable to forming undercoordinated lead ions and halide vacancies, thus triggering the materials' degradation [25]. To passivate surface traps, various reagents [15,18,19,26], including ammonium or halide ions

and other electron-donating ligands, were developed and proven to efficiently increase the PL lifetime of the materials. Those researches indicate that charge carrier dynamics, the photoluminescence quantum yield (PLQY) and the material stability are strongly related to defects on the surface and inside the perovskite bulks.

Though theoretical work has provided many insights on intrinsic defects and extrinsic dopants and their influence on perovskites' optoelectronic properties [27–29], experimental methods have a limited capability to characterize the chemical structure of defect species due to the great variation of defect properties. Therefore, the correlation between specific defects and their influence on devices is still under debate; much progress would be made if one could control the type and concentration of defects in perovskite materials. In this work, we used inert gas nitrogen (N_2) to bring moderate oxidant BQ onto the surface of $MAPbI_3$ and precisely controlled the oxidation reaction under laser irradiation. We used the PL intensity after treatment as an indicator of the concentration of defects, which can be precisely controlled by the laser irradiation time. Perovskites' thin films of different defects concentration manifested different PL responses to oxygen (O_2) and acetone atmosphere. These results prove that the introduced surface vacancies are potential catalysts for redox reactions and indicate that the controllable introduction of defects can help us to gain more insights on defect properties and their impacts on perovskite optoelectronic devices.

2. Materials and Methods

2.1. Sample Preparation

We used a one-step spin-coated deposition method to prepare $MAPbI_3$ thin films [30]. The precursor solution was prepared by adding equimolar methylammonium iodide (CH_3NH_3I , MAI, Xi'an p-OLED, Xi'an, China) and lead iodide (PbI_2 , Sigma-Aldrich (Shanghai, China) Co. Ltd., Shanghai, China) mixtures in γ -butyrolactone (Aladdin, Shanghai, China) and stirring the mixture at 80 °C overnight. $MAPbI_3$ films were fabricated by spin-coating the 40 μ L solution on a cleaned glass substrate (22 \times 22 mm) at 3000 rpm and then annealing at 80 °C for 10 min. The morphology of our samples are polycrystalline thin films of submicron-sized crystals, as shown in Figure S1a. All preparation procedures were carried out in the air. 1,4-benzoquinone was purchased from TCI Shanghai Co. Ltd. (Shanghai, China). During the BQ vapor treatment, to minimize the influence of spatial and sample heterogeneity of trap densities, we always compared adjacent regions on the same sample.

2.2. Photoluminescence Measurements

All PL kinetics and spectra were measured with a home-built wide-field microscope based on an inverted microscope (Olympus IX73, Olympus (China) Co., Ltd., Beijing, China). The PL signal was collected by a dry objective lens (Olympus LUCPlanFI 40 \times , NA = 0.6) and recorded by an EM-CCD camera (iXon Ultra 888, Andor Tech., Belfast, UK) after passing through a 550 nm long-pass filter (ET550lp, Chroma Tech. Crop., Bellows Falls, VT, USA). $MAPbI_3$ samples were excited with a 532 nm diode laser (MGL-III-532, CNI Optoelectronics Tech., Changchun, China). The PL spectrum was measured by adding a grating in front of the detector. During the PL measurement, the atmosphere was switched between N_2 , O_2 and BQ/ N_2 , according to the experimental requirements, and the gas flow rate was controlled by a gas flowmeter.

2.3. Lifetime Measurements

We used a pulsed supercontinuum white laser (WL-SC400, Fianium, Southampton, UK) with AOTFs to obtain a monochromatic light of the selected wavelength. A fast avalanche photodiode (APD, MicroPhoton Devices, Bolzano, Italy) coupled with a time-correlated single photon counting module (PicoHarp 300, PicoQuant, Berlin, Germany) was used for the time-resolved PL decay measurements. The PL decay kinetics were fitted by a bi-exponential decay model and the intensity-averaged lifetimes were extracted from the fitting results.

3. Results and Discussion

3.1. Solution Treatment vs. Vapor Treatment

In our previous work [31], we proved that the treatment of BQ molecules on the perovskite surface can efficiently introduce MA-I double vacancies via an oxidation reaction between BQ and MAI, causing strong PL quenching. However, taking the PL quenching efficiency after the treatment as an index of introduced defect density, it appears the BQ solution treatment is highly variable, especially at a low BQ concentration (Figure S2 in the Supplementary Materials). This is because although solution treatment can degrade perovskite solids easily and effectively when the concentration of BQ is high, there is a large heterogeneity in the amount of BQ at different positions of the film. To better control the amount of BQ and treat the surface more uniformly, in this work, we developed a vapor treatment procedure by using N_2 as the carrier gas to bring BQ molecules onto the perovskite surface.

The vapor treatment procedure is schematically shown in Figure 1a. Dry N_2 goes through a gas-washing bottle containing BQ powders and brings volatile BQ molecules to the perovskite thin film. Taking the PL level in pure N_2 as a reference, we see significant PL quenching once BQ is successfully introduced to the surface, suggesting that the interaction on the gas and solid interface is very effective. The different PL behavior in the N_2 and BQ vapor also indicates that the rapid PL quenching is due to the introduction of BQ vapor instead of a purely photo-induced PL decay, as reported by others [32]. Thanks to the convenience of the vapor treatment, we can monitor the PL response in situ and in real time. According to the PL kinetics during vapor treatment, the time consumed to reach PL quenching saturation is strongly related to the gas flow speed (see Figure 1b) rather than the excitation intensity (Figure S3), indicating that the fast PL quenching effect is mainly related to the amount of BQ on the surface. To further investigate the effect of light irradiation on the quenching effect of BQ, the illumination was turned off before BQ was purged into the container. As shown in Figure 1c, the PL level has already significantly decreased since we turned the light on, which demonstrates that a strong quenching effect can occur without light illumination. However, when we periodically switched the atmosphere between N_2 and BQ (Figure S4), it appears that the fast PL-quenching effect is reversible, unlike the effect of the BQ solution treatment.

To determine how to induce an irreversible effect similar to that with the solution treatment, we carried out BQ vapor treatment cycles (Figure 1d) on the same area with different illumination times. In the first two turns of treatment, once the fast decay stage finished (in 60 s), we kept the sample inside the BQ/ N_2 atmosphere for two more min without light irradiation. After that, we used the N_2 purge for 5 min to remove the intact BQ, then we witnessed a full recovery of the PL level, as expected. However, if we kept the light irradiation for two more min (in the third treatment), N_2 purge would fail to recover the PL intensity. In summary, the adsorption of BQ molecules on the MAPbI₃ thin film can quickly and reversibly quench the PL, but only after enough time of a reaction under the light irradiation would the effect become irreversible, showing that the defect introduction process is a photoinduced reaction.

Here, we can attribute the reversible quenching effect to the electron transfer from the conduction band of MAPbI₃ to BQ. It is reported that charge carriers in MAPbI₃ can facilitate superoxide formation [33] and BQ is an efficient electron acceptor [34] and superoxide scavenger [35]; thus, electron transfer from MAPbI₃ to BQ is possible. Charge transfer between perovskites and BQ would quench the PL of the perovskites; however, once BQ leaves the perovskite surface, the PL level can recover back. Under longer illumination, light-induced charge carriers in perovskites can facilitate the reaction between BQ and MAI, as BQ has been reported to be able to oxidize MAI into volatile methylamine and iodine [36]. Thus, with longer irradiation, PL quenching is irreversible because MA-I double vacancy defects have formed on the surface of MAPbI₃, as discussed elsewhere [31].

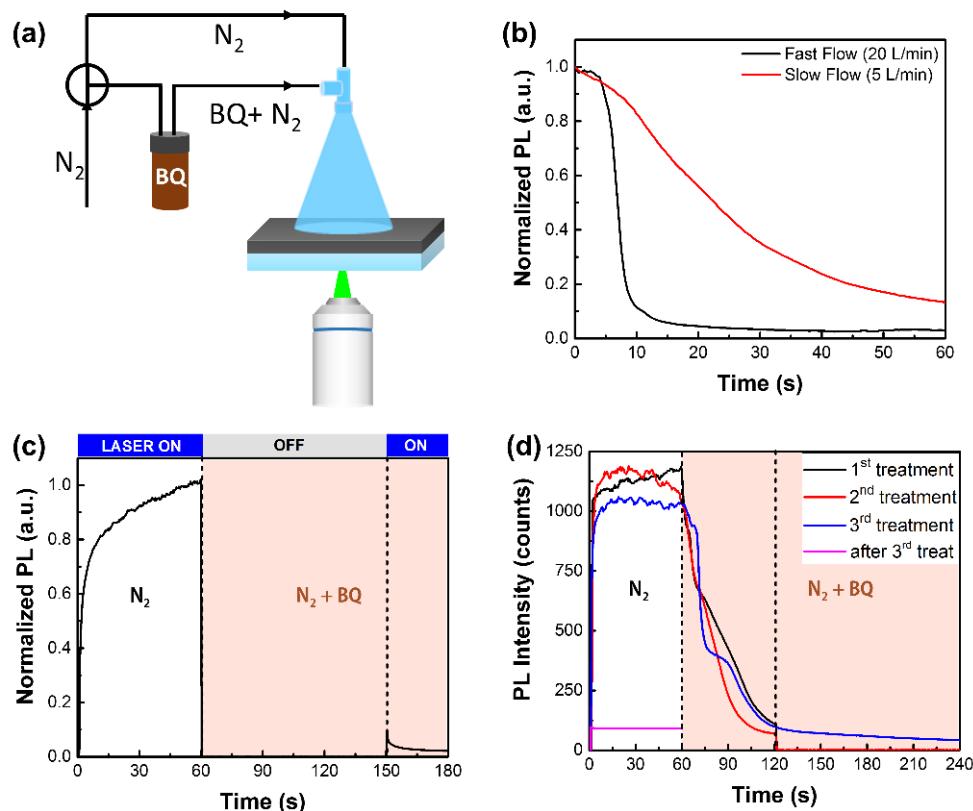


Figure 1. (a) Experimental setup of BQ vapor treatment method. By switching the T-valve, we can change the purge atmosphere between pure N_2 and BQ/N_2 ; (b) PL-quenching kinetics during BQ vapor treatment of different gas flow velocities demonstrate that PL quenching reaches saturation more quickly with faster flow velocity; (c) PL-quenching kinetics show a strong quenching effect of pure BQ adsorption without light irradiation; (d) repeated BQ treatment on the same region for different irradiation time. The sample was illuminated for 60 s in the first and second treatment and 180 s in the third one in BQ/N_2 . Only with longer irradiation in the third treatment could PL not recover back to the original level. All above treatment was under the irradiation of 0.2 W/cm^2 and 532 nm, and the gas flow rate is 5 L per min, besides in Panel b.

3.2. Controllable Surface Defects Introduction

Now, we have a basic understanding of the interaction between BQ molecules and perovskite thin films on the gas and solid interface. By regulating the irradiation duration, we can realize delicate control over the surface defect concentrations. First, we slowed down the gas flow velocity of BQ/N_2 to 5 L per min with an air flowmeter. After that, we can accelerate the reaction by illumination and control the reaction extent with different irradiation durations. Before checking the treatment results, we shut down the laser and used the N_2 purge for 5 min to remove intact BQ molecules. By illuminating four different areas with similar initial PL levels for different durations (60 s, 90 s, 120 s and 150 s), we see in Figure 2 that the PL intensity of $MAPbI_3$ after N_2 purging gradually decreased as the irradiation duration increased. We would like to stress that the four areas are adjacent regions on the same film, and we took signals averaged over tens of micrometers in each area to minimize the influence of heterogeneity in the polycrystalline films. As it is feasible to change the irradiation duration, we can easily control the reaction extent to prepare a series of areas of different PL intensities. In addition, by controlling the light irradiation, we can also selectively treat the material on specific locations.

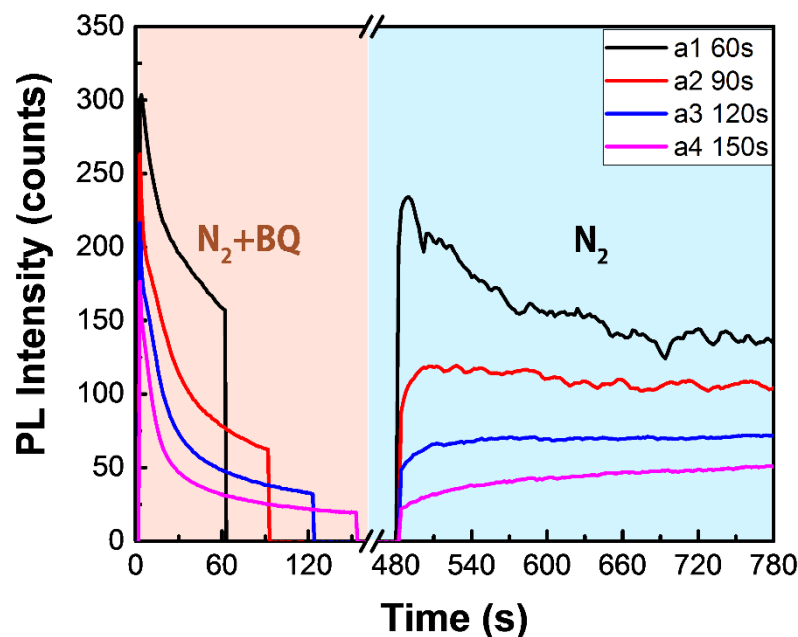


Figure 2. PL kinetics show BQ vapor treatment results with different irradiation durations (at 532 nm) on four areas in the same sample. After BQ vapor treatment, the sample chamber was purged with dry N₂ for 5 min to remove the residual BQ.

To further verify the effect of the BQ vapor treatment, we conducted a series of spectroscopic measurements on the four treated areas. Both the steady-state PL intensity (Figure 3a) and PL decay lifetime (Figure 3b) prove that we prepared four areas of gradually increased degradation extent with consistent variation trends of PL level and lifetime decreasing (in Figure S5a). The PL lifetime measurement is not influenced by the quenching effect of BQ adsorption, as the intact BQ has been removed with the N₂ purge. From the PL decay curves, we can estimate the concentrations of the quenching defects to increase by an order of magnitude from the first to the fourth area (details of simulation can be found in the Supplementary Materials). Although MAPbI₃ thin films experienced significant PL quenching, no spectral shift was observed under different treatment durations (Figure S5b), indicating that the treatment only introduced nonradiative recombination pathways into the crystals rather than destroying them. This can also be verified by no significant variation of the crystal morphology before and after BQ treatment (Figure S1). Furthermore, we measured the PL intensity as a function of the excitation power density, as shown in Figure 3c. The PL intensity (I_{PL}) generally follows a power law relationship against the excitation power density (P_{exc}):

$$I_{PL} = A \times P_{exc}^k \quad (1)$$

In the case of MAPbI₃ measured with a low excitation intensity, the excitation occurs via single photon absorption; thus, the k value indicates the dominant radiative recombination dynamics (monomolecular or bimolecular). At room temperature, the dominant carriers in MAPbI₃ are free charges; thus, the contribution of mono- and bimolecular recombination is related to the trap-filling effect and the density of defects. Wen et al. analyzed in detail that there exists a positive correlation between the density of quenching defects and the k value [37]. We can use the k value to evaluate the density of defect states after BQ vapor treatment, and the fitting results of the power-dependent PL in Figure 3c show that the k value gradually increased in the four areas, indicating a higher defect density induced by the BQ treatment from the first to the fourth area. According to our former results of the BQ solution treatment, the defects introduced by the BQ vapor treatment are probably vacancies of iodine anions (V_{I-}) and methylammonium cations (V_{MA+}) [31].

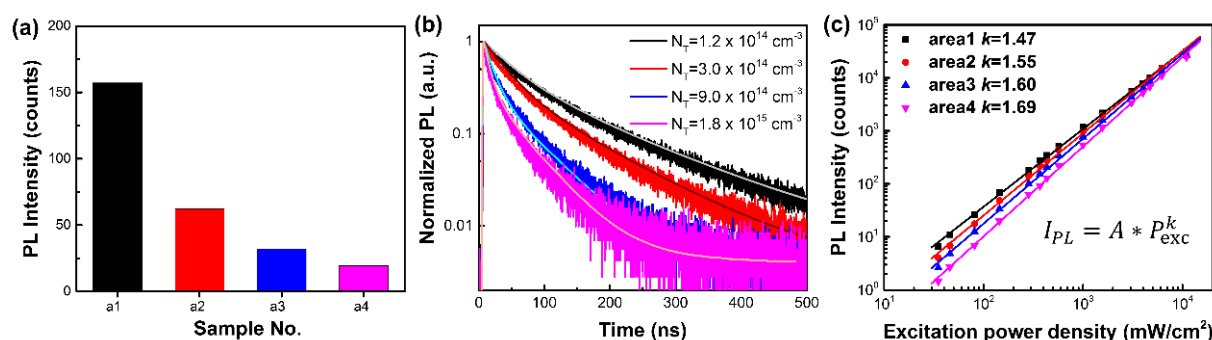


Figure 3. (a) PL intensity of four areas after BQ vapor treatment of different irradiation durations; (b) time-resolved PL decay kinetics and the fitted results of the four areas. Concentrations of deep traps, N_T , evaluated by the PL decay kinetics, are indicated by the legend. The excitation fluence is $2.5 \mu\text{J}/\text{cm}^2$ ($n_0 \sim 3.3 \times 10^{16} \text{ cm}^{-3}$) at 532 nm, 1 MHz; (c) PL intensity (I_{PL}) as a function of excitation intensity (P_{exc}). The dots are experimental results, and the solid lines are fitted results using the power law relationship $I_{PL} = A \times P_{exc}^k$.

According to the above results, we can evaluate the reaction rate of the photo-induced oxidation reaction to get a better control over the defect introduction process. According to the introduced trap density calculated by fitting the PL lifetime (Figure 3b), we evaluated the photo-induced reaction rate on the gas-solid interface to be $3.1 \times 10^{-8} \text{ mol}\cdot\text{L}^{-1}\cdot\text{s}^{-1}$. However, the introduced defects only distributed on the surface region; thus, the actual defect density is even higher than we evaluated here. As reported by Qin et al. [36], the averaged redox reaction rate between BQ and MAI measured by ¹H-NMR is around $1.9 \times 10^{-11} \text{ mol}\cdot\text{L}^{-1}\cdot\text{s}^{-1}$ in the mixture solution of PbI₂, MAI and BQ. We noticed that the reaction on the gas-solid interface is more efficient than the spontaneous reaction in the solution, which might be due to the acceleration of reaction by the light irradiation.

3.3. Impact of Defect Concentration on the PL Response to O₂

The PL quenching and enhancement effect of O₂ on MAPbI₃ have long been debated. Some observed a photoinduced PL enhancement of MAPbI₃ and attributed it to adsorption and chemical reactions involving O₂-related species to passivate defects and suppress nonradiative processes [38,39], while others proposed that superoxide formation would lead to the degradation of MAPbI₃ to PbI₂ [23,40]. Comparing regions with and without light irradiation in the BQ vapor treatment, we see a completely reverse atmospheric effect of O₂, as shown in Figure S6. Furthermore, by preparing areas of different surface defect densities, we simultaneously observed the PL quenching and enhancement effects of O₂ on the same region and compared their different relationships with the density of MA-I double vacancies. The coexistence of the favorable and detrimental effects of the atmosphere are related to the type, concentration and charge states of crystal defects.

As shown in Figure 4a, all four areas treated with BQ vapor show a fast and strong PL-quenching response to O₂. Although the four areas with different surface defect densities show gradually decreasing PL levels in dry N₂, the quenching efficiencies in the O₂ of those areas show almost no difference, indicating that the PL-quenching effect is related to the intrinsic surface structure as synthesized, rather than the MA-I double vacancies introduced by the BQ treatment. Reversible PL quenching by O₂ on the time scale of tens of seconds has been observed by others. Some suggested that O₂ can receive electrons from MAPbI₃ and quench the excited states [41], while others attributed it to the activation of deep defects inside the bandgap [42]. According to previous results [23,31], electron transfer can be facilitated by iodine vacancies. However, in our case, the introduced iodine vacancy has a trivial influence on the PL-quenching process, indicating that this effect is probably not due to O₂ as an electron scavenger on iodine vacancies or any other iodine-related species. Therefore, the most suspicious species inducing PL quenching in O₂ are the Pb-related

species, because BQ has little effect on them; thus, their concentrations would not change much after the treatment.

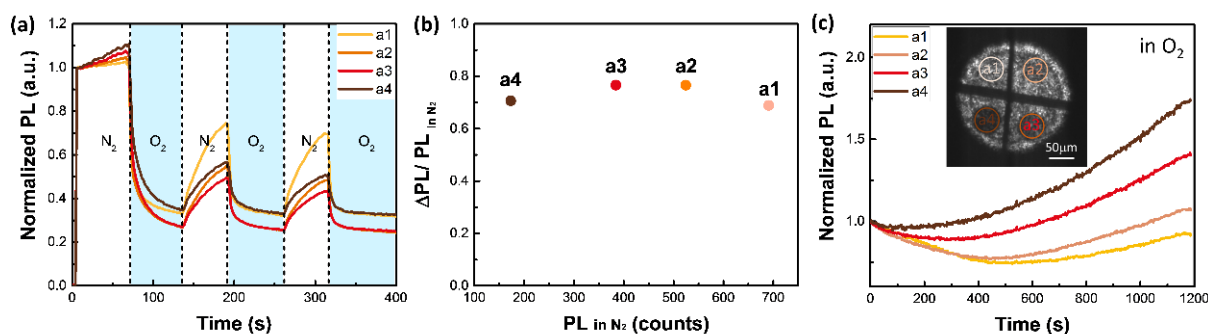


Figure 4. (a) PL-quenching effect and (c) PL-enhancement effect of O₂ in the four BQ-treated areas with gradually increasing surface defect densities from the first to the fourth area; (b) PL-quenching efficiency of O₂ in four areas on the same sample extracted from the data in Panel a. The PL level gradually decreased from the first area to the fourth area.

Although MAPbI₃ shows PL quenching at first, after a longer illumination period, it started showing a PL-enhancement trend in the O₂ atmosphere, as shown in Figure 4c. The PL intensity variation is determined by the competition between PL quenching and PL enhancement. Interestingly, the PL-enhancement rate increases with increasing defect densities from the first to the fourth region. The consistent trends of the surface defect density and PL enhancement rate prove that PL curing is mediated by vacancies introduced by BQ treatment. However, compared to the fast decay (Figure 1b) resulting from BQ adsorption on the MAPbI₃ surface, the PL enhancement is much slower on a time scale of tens to hundreds of min, indicating that the interaction between O₂ and surface defects is more complex than pure adsorption. Previous work from our group [31] and others [39] proposed that the PL curing of O₂ is mediated by iodine vacancies. It was also theoretically proven that O₂ molecules energetically prefer to adsorb on iodine vacancies and can receive electrons from the conduction band to form superoxide species [23,43]. Here comes the controversy that some suggested O₂ adsorption and the formation of superoxide would passivate iodine vacancies and improve the PLQY [39,43], while others proposed that superoxide would cause the degradation of MAPbI₃ and instability of perovskite devices [23,40]. Our experimental results confirmed that O₂ would passivate iodine vacancies and improve the PLQY on a time scale of tens to hundreds of min.

3.4. Impact of Defect Concentration on the Photocatalysis Reaction

Superoxide is a highly reactive oxidizing species; thus, the light-induced formation of superoxide on perovskite surfaces enables the potential application of this material in photocatalysis. In fact, perovskite-type oxides have long been utilized as photocatalysts for CO₂ reduction, water splitting and organic pollutant degradation [27,44,45]. Advantages of metal halide perovskites, i.e., efficient charge separation, strong absorption and suitable bandgap, not only make it a good candidate for solar cells but also for photocatalysis [46]. Our previous work demonstrated that BQ-treated MAPbI₃ can mediate acetone oxidation under light illumination [31]. During the reaction, O₂ molecules adsorb on iodine vacancies and accept electrons, while acetone adsorb on MA⁺ vacancies and accept holes. Here, we compared the photocatalytic reactivity of MAPbI₃ micro-areas with different surface defect densities and illustrated the active sites responsible for charge transfer during photocatalysis.

Taking advantage of the precise control over surface defects via the BQ vapor treatment, we treated the four areas on the same sample in the BQ vapor for different irradiation durations to check their PL response in the mixture of O₂ and acetone. At first, both O₂ and acetone can passivate surface defects, thus inducing PL enhancement. After a while,

PL levels started to decrease and the degradation was irreversible, i.e., the perovskite lattice was destroyed. PL images of the treated areas demonstrated that their PL levels gradually decreased, while the degradation rates gradually increased as the defect density increased from the first to the fourth area, as shown in Figure 5. The correlation between the degradation rate and surface vacancy concentration further confirms that MA-I double vacancies are active sites mediating the charge transfer. Combined with the above results that O₂ can form superoxide on iodine vacancies, more experimental evidence was obtained to prove the Usanovich acid-base passivation mechanism [31] of O₂ and acetone on the MAPbI₃ surface.

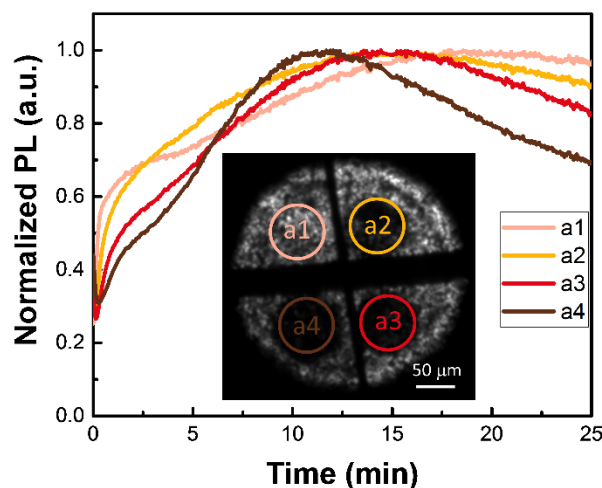


Figure 5. PL responses of the four areas with gradually increasing defect concentration in the mixture of O₂ and acetone. The inset shows the PL image of four areas (a1–a4) whose PL levels gradually decreased after BQ vapor treatment for different irradiation durations. Only the circled regions were treated under laser irradiation.

4. Conclusions

In this work, we developed a vapor treatment method to realize precise control of the defect concentration on the MAPbI₃ surface by a photoinduced chemical reaction with BQ. We found that the adsorption of BQ can cause reversible reduction of the PLQY of MAPbI₃, but only with laser illumination can MA-I double vacancies be introduced as quenchers. Controllable surface modification is facilitated by controlling the duration of light irradiation. The PL response to oxygen and the photocatalysis reaction of oxygen and acetone were checked in areas with different BQ treatments, demonstrating the dependence of the atmospheric effect on the concentration of surface vacancies. Our experimental results distinguished the origins of PL quenching and the enhancement effect of oxygen on MAPbI₃ thin films and identified the defect species responsible for the atmospheric effect. This method also illustrates that defects can also be useful in photocatalysis. In the future, we can apply this method to characterize the chemical nature of the surface defects and build up the correlation of defect structures and the photophysical processes mediated by the defects.

Supplementary Materials: The following supporting information can be downloaded at: <https://www.mdpi.com/article/10.3390/nano12061002/s1>, Figure S1: Morphology of MAPbI₃ thin films; Figure S2: Effects of BQ solution treatment; Figure S3: Dependence of BQ treatment efficiency on excitation intensity; Figure S4: Reversible PL response in N₂ and N₂/BQ mixture; Figure S5: PL spectra before and after the treatment; Figure S6: PL image and response to O₂ and acetone with and without treatment; Figure S7: Estimation of initial carrier density n_0 and the deep trap density N_T .

Author Contributions: Conceptualization, Y.T.; investigation, S.W. and Y.Z.; methodology, D.H.; writing—original draft preparation, S.W.; writing—review and editing, Y.T.; supervision, Y.T.; project administration, Y.T.; funding acquisition, Y.T. All authors have read and agreed to the published version of the manuscript.

Funding: This work is supported by the National Natural Science Foundation of China (NSFC Nos. 22073046 and 62011530133), the Fundamental Research Funds for the Central Universities (020514380256) and the STINT China-Sweden mobility program CH2019-8329. This work is also supported by the Double-Innovation Doctor Program of Jiangsu Province, China (No. JSSCBS20211151) and the Funding for School-level Research Projects of the Yancheng Institute of Technology (xjr2021062).

Institutional Review Board Statement: Not applicable.

Informed Consent Statement: Not applicable.

Data Availability Statement: The data is available on reasonable request from the corresponding author.

Conflicts of Interest: The authors declare no conflict of interest.

References

1. Kovalenko, M.V.; Protesescu, L.; Bodnarchuk, M.I. Properties and Potential Optoelectronic Applications of Lead Halide Perovskite Nanocrystals. *Science* **2017**, *358*, 745–750. [[CrossRef](#)] [[PubMed](#)]
2. Kojima, A.; Teshima, K.; Shirai, Y.; Miyasaka, T. Organometal Halide Perovskites as Visible-Light Sensitizers for Photovoltaic Cells. *J. Am. Chem. Soc.* **2009**, *131*, 6050–6051. [[CrossRef](#)] [[PubMed](#)]
3. Green, M.A.; Ho-Baillie, A.; Snaith, H.J. The Emergence of Perovskite Solar Cells. *Nat. Photonics* **2014**, *8*, 506–514. [[CrossRef](#)]
4. Al-Ashouri, A.; Köhnen, E.; Li, B.; Magomedov, A.; Hempel, H.; Caprioglio, P.; Márquez, J.A.; Morales Vilches, A.B.; Kasparavicius, E.; Smith, J.A.; et al. Monolithic Perovskite/Silicon Tandem Solar Cell with 29% Efficiency by Enhanced Hole Extraction. *Science* **2020**, *370*, 1300–1309. [[CrossRef](#)]
5. Tsai, H.; Shrestha, S.; Vilá, R.A.; Huang, W.; Liu, C.; Hou, C.-H.; Huang, H.-H.; Wen, X.; Li, M.; Wiederrecht, G.; et al. Bright and Stable Light-Emitting Diodes Made with Perovskite Nanocrystals Stabilized in Metal–Organic Frameworks. *Nat. Photonics* **2021**, *15*, 843–849. [[CrossRef](#)]
6. Qin, C.; Sandanayaka, A.S.D.; Zhao, C.; Matsushima, T.; Zhang, D.; Fujihara, T.; Adachi, C. Stable Room-Temperature Continuous-Wave Lasing in Quasi-2D Perovskite Films. *Nature* **2020**, *585*, 53–57. [[CrossRef](#)]
7. Burschka, J.; Pellet, N.; Moon, S.-J.; Humphry-Baker, R.; Gao, P.; Nazeeruddin, M.K.; Grätzel, M. Sequential Deposition as a Route to High-Performance Perovskite-Sensitized Solar Cells. *Nature* **2013**, *499*, 316–319. [[CrossRef](#)]
8. Xing, G.; Mathews, N.; Sun, S.; Lim, S.S.; Lam, Y.M.; Gratzel, M.; Mhaisalkar, S.; Sum, T.C. Long-Range Balanced Electron- and Hole-Transport Lengths in Organic-Inorganic $\text{CH}_3\text{NH}_3\text{PbI}_3$. *Science* **2013**, *342*, 344–347. [[CrossRef](#)]
9. D’Innocenzo, V.; Srimath Kandada, A.R.; De Bastiani, M.; Gandini, M.; Petrozza, A. Tuning the Light Emission Properties by Band Gap Engineering in Hybrid Lead Halide Perovskite. *J. Am. Chem. Soc.* **2014**, *136*, 17730–17733. [[CrossRef](#)]
10. Stranks, S.D.; Eperon, G.E.; Grancini, G.; Menelaou, C.; Alcocer, M.J.P.; Leijtens, T.; Herz, L.M.; Petrozza, A.; Snaith, H.J. Electron-Hole Diffusion Lengths Exceeding 1 Micrometer in an Organometal Trihalide Perovskite Absorber. *Science* **2013**, *342*, 341–344. [[CrossRef](#)]
11. Ponceca, C.S.; Savenije, T.J.; Abdellah, M.; Zheng, K.; Yartsev, A.; Pascher, T.; Harlang, T.; Chabera, P.; Pullerits, T.; Stepanov, A.; et al. Organometal Halide Perovskite Solar Cell Materials Rationalized: Ultrafast Charge Generation, High and Microsecond-Long Balanced Mobilities, and Slow Recombination. *J. Am. Chem. Soc.* **2014**, *136*, 5189–5192. [[CrossRef](#)] [[PubMed](#)]
12. National Renewable Energy Laboratory. Best Research-Cell Efficiency Chart. Available online: <https://www.nrel.gov/pv/cell-efficiency.html> (accessed on 10 February 2022).
13. Rong, Y.; Hu, Y.; Mei, A.; Tan, H.; Saidaminov, M.I.; Seok, S.I.; McGehee, M.D.; Sargent, E.H.; Han, H. Challenges for Commercializing Perovskite Solar Cells. *Science* **2018**, *361*, eaat823. [[CrossRef](#)] [[PubMed](#)]
14. Jeon, N.J.; Noh, J.H.; Kim, Y.C.; Yang, W.S.; Ryu, S.; Seok, S.I. Solvent Engineering for High-Performance Inorganic–Organic Hybrid Perovskite Solar Cells. *Nat. Mater.* **2014**, *13*, 897–903. [[CrossRef](#)] [[PubMed](#)]
15. Lee, J.-W.; Kim, H.-S.; Park, N.-G. Lewis Acid–Base Adduct Approach for High Efficiency Perovskite Solar Cells. *Acc. Chem. Res.* **2016**, *49*, 311–319. [[CrossRef](#)] [[PubMed](#)]
16. Liu, T.; Li, Y.; Feng, S.; Yang, W.; Xu, R.; Zhang, X.; Yang, H.; Fu, W. Incorporation of Nickel Ions to Enhance Integrity and Stability of Perovskite Crystal Lattice for High-Performance Planar Heterojunction Solar Cells. *ACS Appl. Mater. Interfaces* **2020**, *12*, 904–913. [[CrossRef](#)] [[PubMed](#)]
17. Lee, J.-W.; Kim, D.-H.; Kim, H.-S.; Seo, S.-W.; Cho, S.M.; Park, N.-G. Formamidinium and Cesium Hybridization for Photo- and Moisture-Stable Perovskite Solar Cell. *Adv. Energy Mater.* **2015**, *5*, 1501310. [[CrossRef](#)]
18. Jiang, Q.; Zhao, Y.; Zhang, X.; Yang, X.; Chen, Y.; Chu, Z.; Ye, Q.; Li, X.; Yin, Z.; You, J. Surface Passivation of Perovskite Film for Efficient Solar Cells. *Nat. Photonics* **2019**, *13*, 460–466. [[CrossRef](#)]

19. Hu, M.; Nie, R.; Kim, H.; Wu, J.; Chen, S.; Park, B.; Kim, G.; Kwon, H.-W.; Seok, S.I. Regulating the Surface Passivation and Residual Strain in Pure Tin Perovskite Films. *ACS Energy Lett.* **2021**, *6*, 3555–3562. [[CrossRef](#)]
20. Kang, J.; Wang, L.-W. High Defect Tolerance in Lead Halide Perovskite CsPbBr₃. *J. Phys. Chem. Lett.* **2017**, *8*, 489–493. [[CrossRef](#)]
21. Chu, W.; Zheng, Q.; Prezhdo, O.V.; Zhao, J.; Saidi, W.A. Low-Frequency Lattice Phonons in Halide Perovskites Explain High Defect Tolerance toward Electron-Hole Recombination. *Sci. Adv.* **2020**, *6*, aaw7453. [[CrossRef](#)]
22. Park, N.-G.; Segawa, H. Research Direction toward Theoretical Efficiency in Perovskite Solar Cells. *ACS Photonics* **2018**, *5*, 2970–2977. [[CrossRef](#)]
23. Aristidou, N.; Eames, C.; Sanchez-Molina, I.; Bu, X.; Kosco, J.; Islam, M.S.; Haque, S.A. Fast Oxygen Diffusion and Iodide Defects Mediate Oxygen-Induced Degradation of Perovskite Solar Cells. *Nat. Commun.* **2017**, *8*, 15218. [[CrossRef](#)] [[PubMed](#)]
24. Azpiroz, J.M.; Mosconi, E.; Bisquert, J.; De Angelis, F. Defect Migration in Methylammonium Lead Iodide and Its Role in Perovskite Solar Cell Operation. *Energy Environ. Sci.* **2015**, *8*, 2118–2127. [[CrossRef](#)]
25. Sadoughi, G.; Starr, D.E.; Handick, E.; Stranks, S.D.; Gorgoi, M.; Wilks, R.G.; Bär, M.; Snaith, H.J. Observation and Mediation of the Presence of Metallic Lead in Organic–Inorganic Perovskite Films. *ACS Appl. Mater. Interfaces* **2015**, *7*, 13440–13444. [[CrossRef](#)] [[PubMed](#)]
26. Noel, N.K.; Abate, A.; Stranks, S.D.; Parrott, E.S.; Burlakov, V.M.; Goriely, A.; Snaith, H.J. Enhanced Photoluminescence and Solar Cell Performance via Lewis Base Passivation of Organic–Inorganic Lead Halide Perovskites. *ACS Nano* **2014**, *8*, 9815–9821. [[CrossRef](#)] [[PubMed](#)]
27. Chu, Y.; Tan, X.; Shen, Z.; Liu, P.; Han, N.; Kang, J.; Duan, X.; Wang, S.; Liu, L.; Liu, S. Efficient Removal of Organic and Bacterial Pollutants by Ag-La_{0.8}Ca_{0.2}Fe_{0.94}O_{3-δ} Perovskite via Catalytic Peroxymonosulfate Activation. *J. Hazard. Mater.* **2018**, *356*, 53–60. [[CrossRef](#)] [[PubMed](#)]
28. Kim, J.; Lee, S.-H.; Lee, J.H.; Hong, K.-H. The Role of Intrinsic Defects in Methylammonium Lead Iodide Perovskite. *J. Phys. Chem. Lett.* **2014**, *5*, 1312–1317. [[CrossRef](#)]
29. Yin, W.-J.; Shi, T.; Yan, Y. Unique Properties of Halide Perovskites as Possible Origins of the Superior Solar Cell Performance. *Adv. Mater.* **2014**, *26*, 4653–4658. [[CrossRef](#)]
30. Im, J.-H.; Lee, C.-R.; Lee, J.-W.; Park, S.-W.; Park, N.-G. 6.5% Efficient Perovskite Quantum-Dot-Sensitized Solar Cell. *Nanoscale* **2011**, *3*, 4088. [[CrossRef](#)]
31. Yu, Y.; Wan, S.; Hong, D.; Tian, Y. Photo-Induced Dual Passivation via Usanovich Acid–Base on Surface Defects of Methylammonium Lead Triiodide Perovskite. *Phys. Chem. Chem. Phys.* **2018**, *20*, 28068–28074. [[CrossRef](#)]
32. Chen, S.; Wen, X.; Huang, S.; Huang, F.; Cheng, Y.-B.; Green, M.; Ho-Baillie, A. Light Illumination Induced Photoluminescence Enhancement and Quenching in Lead Halide Perovskite. *Sol. RRL* **2017**, *1*, 1600001. [[CrossRef](#)]
33. Feng, X.; Su, H.; Wu, Y.; Wu, H.; Xie, J.; Liu, X.; Fan, J.; Dai, J.; HE, Z. Photon-Generated Carriers Excited Superoxide Species Inducing Long-Term Photoluminescence Enhancement of MAPbI₃ Perovskite Single Crystals. *J. Mater. Chem. A* **2017**, *5*, 12048–12053. [[CrossRef](#)]
34. Wu, K.; Liang, G.; Shang, Q.; Ren, Y.; Kong, D.; Lian, T. Ultrafast Interfacial Electron and Hole Transfer from CsPbBr₃ Perovskite Quantum Dots. *J. Am. Chem. Soc.* **2015**, *137*, 12792–12795. [[CrossRef](#)] [[PubMed](#)]
35. Fónagy, O.; Szabó-Bárdos, E.; Horváth, O. 1,4-Benzoquinone and 1,4-Hydroquinone Based Determination of Electron and Superoxide Radical Formed in Heterogeneous Photocatalytic Systems. *J. Photochem. Photobiol. A Chem.* **2021**, *407*, 113057. [[CrossRef](#)]
36. Qin, C.; Matsushima, T.; Fujihara, T.; Adachi, C. Multifunctional Benzoquinone Additive for Efficient and Stable Planar Perovskite Solar Cells. *Adv. Mater.* **2017**, *29*, 1603808. [[CrossRef](#)] [[PubMed](#)]
37. Wen, X.; Feng, Y.; Huang, S.; Huang, F.; Cheng, Y.-B.; Green, M.; Ho-Baillie, A. Defect Trapping States and Charge Carrier Recombination in Organic–Inorganic Halide Perovskites. *J. Mater. Chem. C* **2016**, *4*, 793–800. [[CrossRef](#)]
38. Tian, Y.; Peter, M.; Unger, E.; Abdellah, M.; Zheng, K.; Pullerits, T.; Yartsev, A.; Sundström, V.; Scheblykin, I.G. Mechanistic Insights into Perovskite Photoluminescence Enhancement: Light Curing with Oxygen Can Boost Yield Thousandfold. *Phys. Chem. Chem. Phys.* **2015**, *17*, 24978–24987. [[CrossRef](#)]
39. Wei, X.; Zhang, Y.; Zheng, T.; Gao, L.; Jiang, J.; Zhao, W.; Liu, H.; Lu, J.; Ni, Z. Competition between Oxygen Curing and Ion Migration in MAPbI₃ Induced by Irradiation Exposure. *J. Phys. Chem. Lett.* **2020**, *11*, 8477–8482. [[CrossRef](#)]
40. Senocrate, A.; Acartürk, T.; Kim, G.Y.; Merkle, R.; Starke, U.; Grätzel, M.; Maier, J. Interaction of Oxygen with Halide Perovskites. *J. Mater. Chem. A* **2018**, *6*, 10847–10855. [[CrossRef](#)]
41. Nandayapa, E.R.; Hirslandt, K.; Boeffel, C.; Unger, E.L.; List-Kratochvil, E.J.W. Unraveling Reversible Quenching Processes of O₂, N₂, Ar, and H₂O in Metal Halide Perovskites at Moderate Photon Flux Densities. *Adv. Opt. Mater.* **2021**, *9*, 2001317. [[CrossRef](#)]
42. Mantulnikovs, K.; Glushkova, A.; Kollar, M.; Forro, L.; Horvath, E.; Sienkiewicz, A. Differential Response of the Photoluminescence and Photocurrent of Polycrystalline CH₃NH₃PbI₃ and CH₃NH₃PbBr₃ to the Exposure to Oxygen and Nitrogen. *ACS Appl. Electron. Mater.* **2019**, *1*, 2007–2017. [[CrossRef](#)]
43. Brenes, R.; Eames, C.; Bulović, V.; Islam, M.S.; Stranks, S.D. The Impact of Atmosphere on the Local Luminescence Properties of Metal Halide Perovskite Grains. *Adv. Mater.* **2018**, *30*, e1706208. [[CrossRef](#)] [[PubMed](#)]
44. Xie, K.; Umezawa, N.; Zhang, N.; Reunchan, P.; Zhang, Y.; Ye, J. Self-Doped SrTiO_{3-δ} Photocatalyst with Enhanced Activity for Artificial Photosynthesis under Visible Light. *Energy Environ. Sci.* **2011**, *4*, 4211. [[CrossRef](#)]

45. Kato, H.; Asakura, K.; Kudo, A. Highly Efficient Water Splitting into H₂ and O₂ over Lanthanum-Doped NaTaO₃ Photocatalysts with High Crystallinity and Surface Nanostructure. *J. Am. Chem. Soc.* **2003**, *125*, 3082–3089. [[CrossRef](#)]
46. Huang, H.; Pradhan, B.; Hofkens, J.; Roeffaers, M.B.J.; Steele, J.A. Solar-Driven Metal Halide Perovskite Photocatalysis: Design, Stability, and Performance. *ACS Energy Lett.* **2020**, *5*, 1107–1123. [[CrossRef](#)]